

Enhanced optical transmission, beaming and focusing through a subwavelength slit under excitation of dielectric waveguide modes

This article has been downloaded from IOPscience. Please scroll down to see the full text article.

2009 J. Opt. A: Pure Appl. Opt. 11 125702

(<http://iopscience.iop.org/1464-4258/11/12/125702>)

[The Table of Contents](#) and [more related content](#) is available

Download details:

IP Address: 150.244.9.175

The article was downloaded on 27/10/2009 at 08:42

Please note that [terms and conditions apply](#).

Enhanced optical transmission, beaming and focusing through a subwavelength slit under excitation of dielectric waveguide modes

A Yu Nikitin^{1,2}, F J García-Vidal³ and L Martín-Moreno¹

¹ Instituto de Ciencia de Materiales de Aragón and Departamento de Física de la Materia Condensada, CSIC-Universidad de Zaragoza, E-50009, Zaragoza, Spain

² A Ya Usikov Institute for Radiophysics and Electronics, Ukrainian Academy of Sciences, 61085 Kharkov, Ukraine

³ Departamento de Física Teórica de la Materia Condensada, Universidad Autónoma de Madrid, E-28049 Madrid, Spain

E-mail: alexeynik@rambler.ru

Received 10 August 2009, accepted for publication 28 August 2009

Published 21 September 2009

Online at stacks.iop.org/JOptA/11/125702

Abstract

We explore the transmission and beaming properties of a single subwavelength slit flanked by a finite array of indentations made on a thick metallic film for both s- and p-polarizations. If a dielectric slab is placed onto the metal film, excited dielectric waveguide modes drastically change the diffraction of a plane wave. We show that if a dielectric slab is placed at the incoming face of the film, the transmission can be greatly enhanced for wavelengths which are close to the Bragg reflection condition. For the same wavelengths, the waveguide modes can be redirected into a highly collimated beam within a few degrees; however, in this case, the slab must be placed at the outgoing face of the film.

Keywords: enhanced transmission, beaming, focusing, surface waves, waveguide modes

(Some figures in this article are in colour only in the electronic version)

1. Introduction

The diffraction of optical waves by nano-apertures has been a subject of intense research over the last decade. The latest achievements in both theoretical and experimental studies demonstrate that, transmission characteristics of the structure suffer drastic changes whenever bounded electromagnetic (EM) waves are involved in the diffraction by subwavelength apertures. For instance, a periodic array of subwavelength slits in a metal film shows, apart from Fabry–Perot-like peaks, a significant enhancement of the transmission (compared to the single slit) at certain wavelengths [1–6]. These resonances have been associated with localized surface modes that could be both spoof and conventional surface plasmon-polaritons (SPPs) supported by the corrugated metallic surfaces [7–9]. Since SPPs are p-polarized, only the p-polarization component

of the incident radiation can be resonantly transmitted through subwavelength slits. In this sense, subwavelength slit arrays act as polarization selectors: the penetration of the s-polarized component of the field is suppressed. However, if the dielectric layers are deposited onto the metal film, the structure supports s-polarization dielectric waveguide modes (DWMs). DWMs then play the part of SPPs and s-polarized radiation can also be resonantly transmitted through subwavelength slits [10].

Another attractive configuration is a single slit in a metal film flanked by corrugations. The periodic location of the corrugations from each side of the slit results in the formation of electromagnetic surface resonances that can provide enhanced transmission [11–14] and beaming [15–21] of p-polarized radiation. Similar effects have been found for the same geometrical structures with other physical properties: for matter [22] and sonic waves [23, 24].

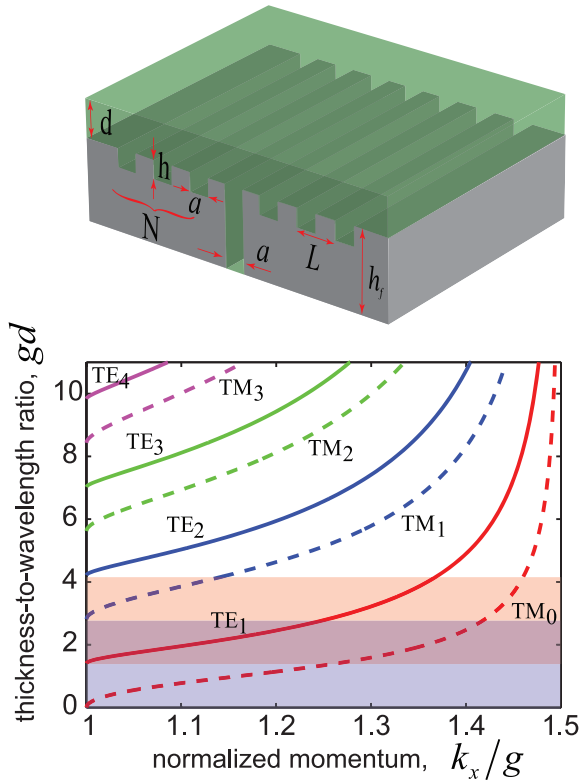


Figure 1. The geometry of the studied system and the dispersion curves of both TM (dashed lines) and TE (continuous lines) DWMs existing in the glass slab ($\epsilon = 2.25$) placed onto the metal surface. The highlighted regions represent single-mode regimes.

In this paper we study the transmission of the plane electromagnetic wave through the slit drilled in a metal film with additional dielectric layers bounding to the film faces. The slit is surrounded by indentations so that resonance effects due to the launching and re-emission of DWMs take place [25]. Since the DWMs are supported both for p- and s-polarizations, the enhanced transmission and collimation of the radiation in the far- and near-field regions are achieved for both polarizations.

2. Spectral properties

Consider a plane monochromatic wave normally incident onto the perfect electric conductor (PEC) metal film of thickness h_f with $2N$ indentations flanking symmetrically a slit of width a from each side, see figure 1. The indentations, of depth h and width a , are placed either on the incoming face of the film, or on the outgoing one. The distance between the indentations L (the period) is equal to the distance from the center of the slit to the center of the first indentation. The metal film bounds to the dielectric layer of thickness d with dielectric permittivity ϵ . Due to the in-plane geometry, s- and p-polarizations can be treated separately (there is no cross-conversion).

To solve the EM problem, we use the coupled mode method [11, 15, 22], see appendix A. The fields in the dielectric slab and dielectric half-spaces are projected onto a basis of plane waves, and inside the slit and the cavities they

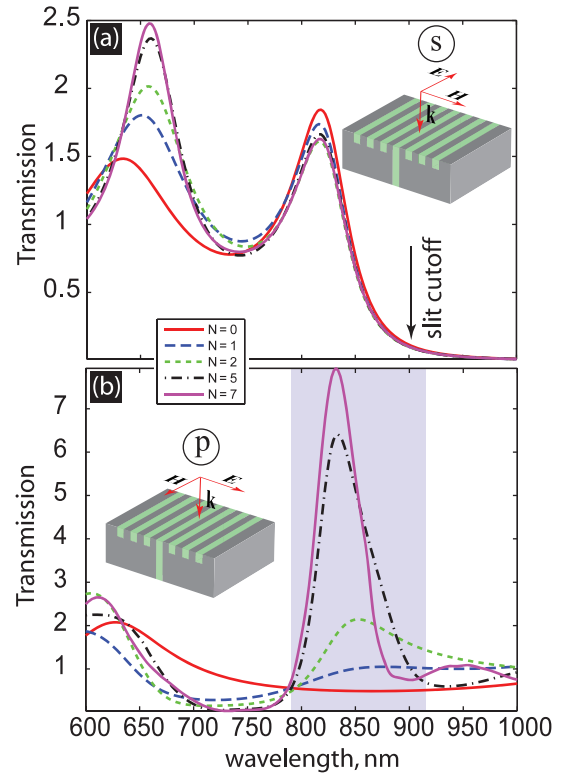


Figure 2. Transmission spectra for s-polarized (a) and for p-polarized (b) waves as a function of the number of indentations N , placed on the side of incidence. In (a) $h_f = 370$ nm, $h = 200$ nm, $L = 636$ nm, $a = 300$ nm and in (b) $h_f = 370$ nm, $h = 100$ nm, $L = 750$ nm, $a = 100$ nm.

are projected onto a set of waveguide modes. Then the fields in different regions are matched on the surfaces and the system of equations for the modal amplitudes is derived. The solution of this system of equations gives the modal amplitudes, from where the scattering parameters (transmittance, reflectance, scattering cross-section, etc) can be computed, see appendix A. Throughout, we consider a normal incidence illumination by a monochromatic plane wave with wavelength λ .

Let us start by considering the transmission spectra of the slit symmetrically flanked by indentations in the film placed between two semi-infinite vacuum media. The indentations are placed in the side of incidence. We assume that both the slit and the indentations are filled by a dielectric with refractive index 1.5 and that there is no additional dielectric layer ($d = 0$). The transmittance spectra, normalized to the slit width, for different numbers of indentations are shown in figure 2. An essential difference between the spectra of p- and s-polarized radiation is already noticeable for a single slit without corrugation. While for the p-polarization the spectra are always composed of interlaced maxima associated with the Fabry–Perot slit waveguide resonances [15], for s-polarization the resonance maxima change to a rapid falling [25, 26]. Such a distinct spectral behavior is due to the existence of the slit mode cutoff at the wavelength λ_c for s-polarization. For the lowest slit mode TE₁, the cutoff wavelength λ_c is given by $\lambda_c = 2a\sqrt{\epsilon_s}$, where ϵ_s is the dielectric permittivity of the slit

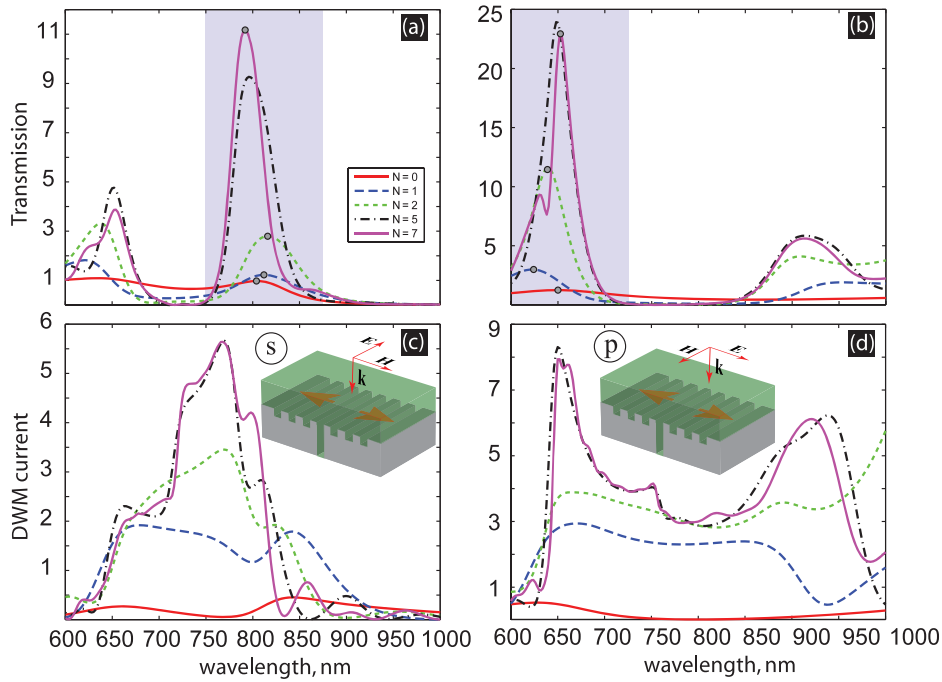


Figure 3. Normalized to the slit width transmission spectra ((a), (b)) and DWM current ((c), (d)) for s- and p-polarized waves. In all panels $h_f = 370$ nm, $d = 250$ nm. In ((a), (c)) $h = 200$ nm, $a = 300$ nm, $L = 636$; in ((b), (d)) $h = 100$ nm, $a = 100$ nm, $L = 550$ nm.

and indentations filling. Therefore, for a 300 nm slit width filled by glass, $\lambda_c = 900$ nm, see figure 2(a).

Once the cavities appear on the incoming face of the metal film, EM resonances associated with them have a significant effect on the transmittance spectra for p-polarization. The resonances are originated by the interplay between the groove cavity mode and the in-phase groove re-emission mechanisms. The standard Fano-type resonance transmission peaks are clearly seen close to $\lambda \simeq 850$ nm (shaded region in figure 2(b)). Increasing the number of indentations, the resonance becomes narrower, indicating that a spoof plasmon mode formation takes place. With the presence of indentations, the transmittance value is increased approximately by an order of magnitude as compared to the transmittance value for the single slit. In contrast, the s-polarization case does not present such an enhancement, see figure 2(a). With the growing number of indentations, the transmission coefficient increases close to the Fabry–Perot peaks but not as strongly as for the p-polarization. This could have been expected since for the in-plane geometry the corrugated metal interface does not support EM eigenmodes.

To enhance the transmission for s-polarization, the waveguiding dielectric layer can be used in order to involve the DWMs [10]. The transmission spectra for the slit in the metal film bounded to the waveguiding layer are shown in figures 3(a) and (b) for s- and p-polarizations respectively. Distinct curves correspond to different numbers of indentations N surrounding the slit. The resonant peaks growing with the increase of the number of indentations are clearly seen both for s- and p-polarization. In order to interpret the resonant behavior of the spectra, the influence of the DWM of the bounding dielectric modes should be analyzed.

According to the DWM dispersion (see figure 1), the interval of the single-mode regime is $gd \simeq [1.43, 4.21]$ for the TE case and $gd \simeq [0, 2.81]$ for the TM case (TM DWMs do not present cutoff), where $g = 2\pi/\lambda$. The thickness $d = 250$ nm corresponds to the wavelength interval $\lambda \simeq [372.68, 1097.84]$ nm for TE DWMs and $\lambda \simeq [581.78, \infty]$ nm for TM DWMs. Therefore, for the chosen glass layer thickness, only one DWM can be supported for the wavelength interval in figure 3. For each wavelength, the DWM is launched due to the diffraction on the slit and indentations. The DWM can be reflected and emitted by them, and the efficiency of the interaction at a certain wavelength depends upon the location of the indentations. Close to the wavelength λ_n of the n th peak, the DWM is efficiently reflected back from the gratings to the slit, originating the field enhancement inside the latter. The opposite side of the slit plays the role of the emitting aperture and generates the transmitted out-of-plane radiation. The wavelength of the transmission maximum is approximately defined by the Bragg reflection condition $\lambda_n = 2Lq_w/n$, where L is the period, $q_w = k_{xw}/g$ is the normalized momentum of the DWM, and n numerates the band-gaps of the reminiscent periodic structure. In fact, the resonance condition is somewhat more complicated due to both the dispersion of the DWM [$q_w = q_w(\lambda)$] and the radiation losses and finiteness of the structure. We would like to point out that while for s-polarization the transmission peaks are solely due to DWM launching, for p-polarization DWM resonances are mixed up with the spoof SPPs.

Figures 3(c) and (d) illustrate the spectra of the DWM energy flux. The dependency on wavelength is strongly non-monotonic. Close to the transmission peaks, the DWM current also increases significantly. This is due to the in-phase

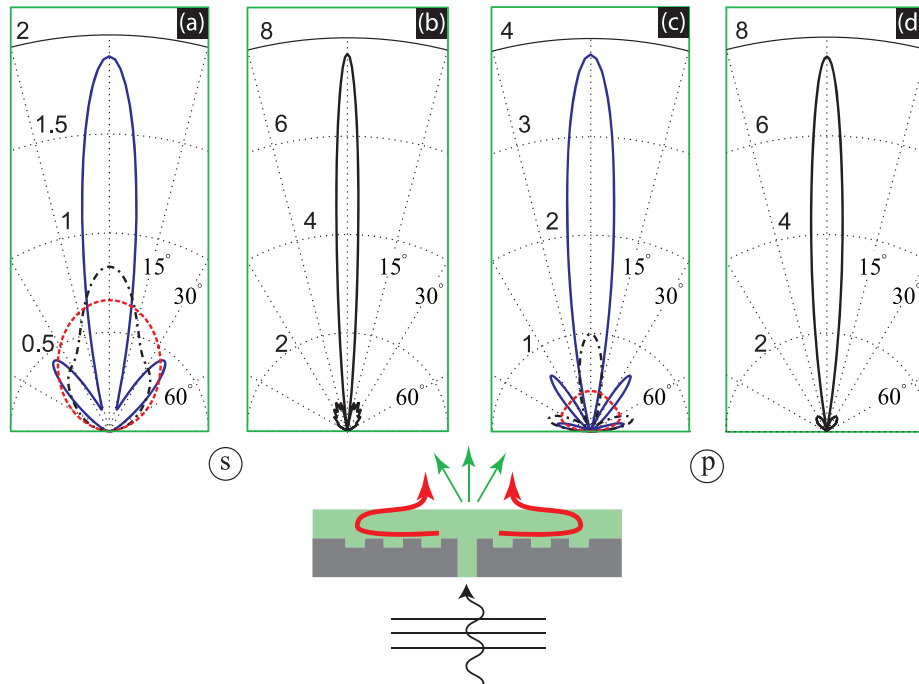


Figure 4. Scattering cross-sections in polar coordinates. The parameters of the structure are the same as in figure 3 for s- and p-polarizations respectively. In (a) the number of indentations from each side of the slit is $N = 0$ at $\lambda = 804$ nm (dashed line), $N = 1$ at $\lambda = 812$ nm (dash-dotted line) and $N = 2$ at $\lambda = 816$ nm (continuous line); in (b) $N = 7$ at $\lambda = 792$ nm. In (c) $N = 0$ at $\lambda = 650$ nm (dashed line), $N = 1$ at $\lambda = 622$ nm (dash-dotted line) and $N = 2$ at $\lambda = 640$ nm (continuous line); in (d) $N = 7$ at $\lambda = 652$ nm. The wavelengths correspond to the gray circle markers located on the spectral curves of figures 3(a) and (b).

conversion of the incident plane wave into the DWMs by the arrays of indentations: the part of the DWM energy that is not transmitted through the slit is taken away along the interface forming the DWM currents.

3. Beaming characteristics

The transmitted radiation cross-section $S_r(\theta)$ is given by the field distribution on the slit and the cavities placed on the outgoing face of the film. More precisely, the field is given by the convolution of the electromagnetic propagator with the fields of all the exit apertures. If the indentations are not present on the outgoing face of the slit, the cross-section for s-polarization is reminiscent of the radiation pattern of a two-dimensional dipole, $S_r(\theta) \sim \cos^2 \theta$, where θ is a polar angle counted from the normal to the film face. For p-polarization, the radiation pattern is almost isotropic, $S_r(\theta) \sim \text{const}$. The presence of the dielectric layer on the outgoing face of the film deforms the cross-section and the diffraction shadow appears. The energy flux inside the diffraction shadow is mainly provided by DMW channels.

When the indentations appear on the exit face of the film, the output side of the slit diffracts a transmitted field into the dielectric regions and into the cavities. The cavities in turn, scatter radiation either into other indentations or out-of-plane (or both). Therefore, the indented surface presents a set of localized emitters with self-consistently formed phases and amplitudes. The radiation pattern then depends upon the phase and the amplitude differences between the slit and the indentation regions.

An interesting situation occurs when the diffracted beam generates a leaky surface mode. On these conditions, the beams from all grooves and the slit are in phase. The leaky mode can be formed at the exit side, if the surface has a sufficient number of periodically-located grooves. Actually, if the structure does not have a waveguiding layer, the modes (both leaky and non-leaky) can appear only with the presence of the grooves. The field of the leaky mode has some radiative components through which the mode loses the energy by radiating in certain directions. These directions correspond approximately to the propagation directions of the homogeneous diffracted plane waves that appear in the case of the infinite periodic structure (when the number of indentations tends to infinity). The tangential components of the wavevectors of these plane waves are expressed as $k_{nx} = \pm k_w + nG$ ($k_{nx} < g$), where k_w is the mode wavevector x -component, $G = 2\pi/L$ is the modulus of the shorter Bragg vector, n is an integer, and \pm defines the propagation direction of the surface mode. Then the angles $\theta_n^\pm = \arcsin(\pm q_w + n\lambda/L)$ provide the beaming directions [15, 20], that is, the directions corresponding to the radiation pattern maxima.

The beaming effect in the normal direction $\theta = 0$ is illustrated in figure 4. The computed examples correspond exactly to the structures shown in figure 3, but with the incidence from the other side of the film. The beaming wavelengths coincide with those for the resonant transmission peak, where the surface modes are formed. As seen in figure 4, the scattering cross-sections are highly directional at the wavelengths corresponding to the spectra maxima within the shaded regions in figures 3(a) and (b). The beaming intensity

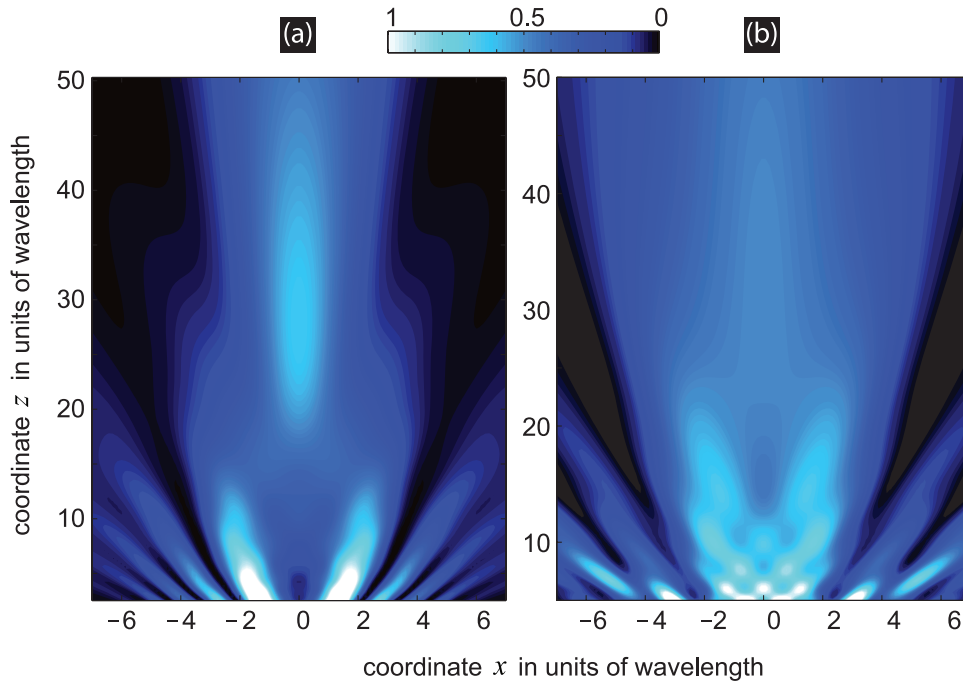


Figure 5. Field intensity spatial distribution. (a) The parameters of the structure for s-polarization are the same as in figures 3(a) and (c). The number of indentations from each side of the slit is $N = 7$; the wavelength is $\lambda = 792$ nm. (b) The parameters are the same as in figures 3(b) and (d), except for the dielectric slab thickness which is $d = 648$ nm; $N = 7$, $\lambda = 656$ nm. The fields are normalized to their maximal values in the shown region.

increases with the number of indentations and saturates after $N \sim 10$.

4. Focusing of the field

The resonant excitation of the bound mode can also lead to the focusing of the field in the output region for the wavelengths at which beaming and enhanced transmission appear. The long focus (of several tens of wavelengths) is seen in figure 5, where the spatial electric field modulus distribution is plotted. For s-polarization, the chosen wavelength was 792 nm, which provides the maximal transmission for the inverse configuration with 7 indentations from each side of the slit. For p-polarization, however, the focus is better exhibited when several DWMs are excited simultaneously. We have chosen the dielectric layer thickness $d = 648$ nm so that the layer supports 3 DWMs (TM_0 , TM_1 , TM_2 , see figure 1) at the resonant wavelength $\lambda = 656$ nm ($gd \simeq 6.21$).

We would like to stress that if both output and input surfaces are corrugated, then the amplitude of the collimated beam and the field in the focus can be increased by orders of magnitude. This occurs since the beaming is accompanied by the enhanced transmission, and these two phenomena act independently.

5. Concluding remarks

We have theoretically shown that the transmission of both s-polarized and p-polarized waves through a single subwavelength slit can be enhanced when a waveguiding

dielectric layer is placed at the incoming face of the film and the aperture is periodically flanked by indentations. If the wave is incident from the other side of the film (so that the output surface is corrugated), the structure displays both beaming and lensing effects. All these phenomena are due to the formation of bounded EM waves: DWMs for the s-polarization and both spoof SPP modes and DWMs for p-polarization.

Such sandwiched structures are possible candidates to form the part of detectors and other optical devices, where a strong film collimation and enhancement is needed.

Acknowledgments

The authors thank Ross Stanley for useful discussions. Financial support is acknowledged from EU project 'PLEAS' FP6-2006-IST-034506, the Spanish Ministry of Science project No. MAT2009-06609-C02 and Spanish MCyT project FIS2006-10045. AYN acknowledges MICINN for a Juan de la Cierva Grant.

Appendix A. Theoretical formalism

Let us briefly describe the coupled mode method that we have used to treat our problem. The geometry is shown in figure A.1. The regions in the dielectric half-spaces are labeled as '1', '5' and inside the additional dielectric layers as '2', '4'. Let the region '1' be the half-space where the incident wave comes

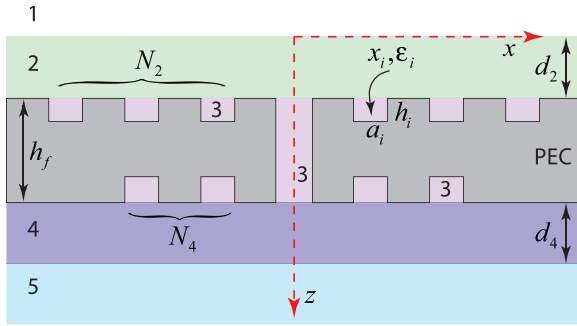


Figure A.1. The geometry of the problem.

from. The fields inside these regions can be represented as

$$\begin{aligned}
 |\mathbf{E}_1(z)\rangle &= e^{ik_{z0}z}|\kappa_0\rangle + \sum_k r_\kappa e^{-ik_{z1}z}|\kappa\rangle, \\
 |\mathbf{E}_2(z)\rangle &= \sum_k [\rho_{k2}^+ e^{ik_{z2}(z-d_2)} + \rho_{k2}^- e^{ik_{z2}(d_2-z)}]|\kappa\rangle, \\
 |\mathbf{E}_4(z)\rangle &= \sum_k [\rho_{k4}^+ e^{ik_{z4}(z-d_2-h_f)} + \rho_{k4}^- e^{ik_{z4}(h_f+d_2-z)}]|\kappa\rangle, \\
 |\mathbf{E}_5(z)\rangle &= \sum_k t_\kappa e^{ik_{z5}(z-d_2-h_f-d_4)}|\kappa\rangle.
 \end{aligned} \tag{A.1}$$

Here $k_{zl} = \sqrt{\epsilon_l g^2 - k^2}$ is the z -component of the wavevector inside the ' l 'th dielectric media; the notation $|\kappa\rangle$ (where $\kappa = (k, l)$) implies the mode representation in Dirac's notations so that $\langle \mathbf{r}|\kappa\rangle$ provides the coordinate representation of a bi-vector ($\langle \kappa|\mathbf{r}\rangle = \langle \mathbf{r}|\kappa\rangle^*$, where $*$ means complex conjugate) having x and y components. The latter has the following form for s- and p-polarization:

$$\begin{aligned}
 s: \langle \mathbf{r}|\kappa\rangle &= \frac{e^{ikx}}{\sqrt{2\pi}} \begin{pmatrix} 0 \\ 1 \end{pmatrix}, \\
 p: \langle \mathbf{r}|\kappa\rangle &= \frac{e^{ikx}}{\sqrt{2\pi}} \begin{pmatrix} 1 \\ 0 \end{pmatrix}.
 \end{aligned} \tag{A.2}$$

The symbol of the summation represents the integral over the whole continuum of k : $\sum_k \equiv \int dk$. The mode $|\kappa_0\rangle$ related to the incident wave will be further specified.

Inside the cavities, the field is represented in terms of the modes of the infinite metal waveguide

$$|\mathbf{E}_3(z)\rangle = \sum_\alpha [A_\alpha^+ e^{ik_{z\alpha}(z-d_\alpha)} + A_\alpha^- e^{ik_{z\alpha}(d_\alpha-z)}]|\alpha\rangle, \tag{A.3}$$

where for the indentation bounding to the layer '2' $d_\alpha = d_2$, for that bounding to the layer '4' $d_\alpha = d_2 + h_f$ and for the slit $d_\alpha = h_f$. The coordinate representation of the cavity modes $|\alpha\rangle$ (where the Latin marker $\alpha = (m, i)$ includes the mode order m , and the index i characterizing the position of the cavity x_i , the permittivity of the cavity filling ϵ_i , the width a_i and the height h_i) reads

$$\begin{aligned}
 \text{TE: } \langle \mathbf{r}|\alpha\rangle &= c_\alpha \begin{pmatrix} 0 \\ 1 \end{pmatrix} \sin \left[q_\alpha \left(x - x_i + \frac{a_i}{2} \right) \right], \\
 \text{TM: } \langle \mathbf{r}|\alpha\rangle &= c_\alpha \begin{pmatrix} 1 \\ 0 \end{pmatrix} \cos \left[q_\alpha \left(x - x_i + \frac{a_i}{2} \right) \right].
 \end{aligned} \tag{A.4}$$

Here $q_\alpha = m\pi/a_i$. The cavities are numerated so that $i = 0$ labels the slit. The normalizing constants are $c_\alpha = \sqrt{2/a_i}$ for the TE case and for the TM case if $m \neq 0$; $c_\alpha = 1/\sqrt{a_i}$ for TM modes under $m = 0$. The z -propagation constants of both types of modes read $k_{z\alpha} = \sqrt{g^2 \epsilon_i - q_\alpha^2}$. Representation of the modes (A.2), (A.4) provides their orthogonality: $\langle \alpha|\alpha'\rangle = \delta_{\alpha,\alpha'}$, $\langle \kappa|\kappa'\rangle = \delta_{\kappa,\kappa'}$, where each projection is given by the integration over the coordinate x : e.g. $\langle \alpha|k\rangle = \int dx \langle \alpha|\mathbf{r}\rangle \langle \mathbf{r}|k\rangle$.

Matching the fields on the interfaces, we arrive at a system of linear equations for the modal amplitudes

$$\begin{aligned}
 \sum_{\beta'} G_{\beta\beta'}^{12} E_{\beta'} + \sigma_\beta E_\beta + \delta_{i,0} g_\beta E'_\beta &= I_\beta, \\
 \sum_{\gamma'} G_{\gamma\gamma'}^{45} E'_{\gamma'} + \sigma_\gamma E'_\gamma + \delta_{i,0} g_\gamma E_\gamma &= 0.
 \end{aligned} \tag{A.5}$$

The indices β correspond to both the modes of the indentations bounding to the layer '2' and to the slit modes ($i = 0$), while the indices γ mark both the set of modes of the indentations bounding to the layer '4' and the slit modes as well. The renormalized modal amplitudes are introduced as follows

$$\begin{aligned}
 i \neq 0: \begin{cases} E_\beta = (A_\beta^+ + A_\beta^-), \\ E_\gamma \equiv E'_\gamma = -(A_\gamma^+ + A_\gamma^-), \end{cases} \\
 i = 0: \begin{cases} E_\alpha = A_\alpha^+ + A_\alpha^-, \\ E'_\alpha = -(A_\alpha^+ e_\alpha + A_\alpha^- e_\alpha^{-1}), \end{cases}
 \end{aligned} \tag{A.6}$$

with $e_\alpha = \exp(ik_{z\alpha}h_i)$, $h_0 \equiv h_f$. The boundary conditions on the bottom of the indentations provide the relation between amplitudes of the backwardly and forwardly propagating waves inside the slit: $A_\beta^- = -A_\beta^+ e_\beta^2$ and $A_\gamma^- e_\gamma^2 = -A_\gamma^+$. We see from equation (A.5) that the modes of the 'upper' and 'lower' indentations are coupled through the slit modes.

The coefficients g_α that describe the coupling between the input and output sides of the slit and the coefficients σ_α arising from the reflection of the waveguide mode at the openings are given by

$$g_\alpha = \frac{2Z_\alpha}{e_\alpha - e_\alpha^{-1}}, \quad \sigma_\alpha = Z_\alpha \frac{e_\alpha + e_\alpha^{-1}}{e_\alpha - e_\alpha^{-1}}, \tag{A.7}$$

where $Z_\alpha = k_{z\alpha}/g$ (TE) and $Z_\alpha = g\epsilon_i/k_{z\alpha}$ (TM) are the cavity waveguiding mode admittances.

The tensor elements $G_{\alpha\alpha'}^{ln}$ ($l = 1, 5$; $n = 2, 4$) present the summation of the projections of the modes over all k -states

$$G_{\alpha\alpha'}^{ln} = \sum_k Z_{kl} \frac{f_{kln}^+}{f_{kln}^-} \langle \alpha|k\rangle \langle k|\alpha'\rangle, \tag{A.8}$$

where $Z_{kl} = k_{zl}/g$ (TE), $Z_{kl} = g\epsilon_l/k_{zl}$ (TM) are the free-space mode admittances in l th dielectric media. The coefficients f_{kln}^\pm related to the reflections inside the waveguiding layers are

$$\begin{aligned}
 f_{kln}^+ &= \cos \phi_n - i \frac{Z_{kl}}{Z_{kn}} \sin \phi_n, \\
 f_{kln}^- &= i \sin \phi_n - \frac{Z_{kl}}{Z_{kn}} \cos \phi_n,
 \end{aligned} \tag{A.9}$$

with $\phi_n = k_{zn}d_n$. Notice that the relation $f_{kln}^- = 0$ defines the eigenmodes of our sandwiched system without corrugations. The integration over x in the mode projections is easily performed analytically and has the following form

$$\begin{aligned} \text{TE: } \langle \alpha | k \rangle &= c_\alpha \sqrt{\frac{2}{\pi}} \frac{q_\alpha S_{k\alpha}}{q_\alpha^2 - k^2} e^{ikx_i}, \\ \text{TM: } \langle \alpha | k \rangle &= c_\alpha \sqrt{\frac{2}{\pi}} \frac{k S_{k\alpha}}{q_\alpha^2 - k^2} e^{ikx_i}, \end{aligned} \quad (\text{A.10})$$

where for the TE case

$$S_{k\alpha} = \begin{cases} \cos(ka_i/2), & m\text{-odd,} \\ -i \sin(ka_i/2), & m\text{-even,} \end{cases} \quad (\text{A.11})$$

and for the TM case the rhs of equation (A.11) must be multiplied by $-i$.

The rhs term I_β in (A.5) reads

$$I_\beta = -\frac{2Z_{k_01}}{f_{k_021}^+} \langle \beta | k_0 \rangle, \quad (\text{A.12})$$

where k_0 is the x -component of the incident wave wavevector. The mode $|\kappa_0\rangle$ is defined analogously to equation (A.2), but has an additional factor $c_0 = \sqrt{2\pi/(Z_{k_01}a_0)}$ so that the Poynting vector flux of the incident wave through the area of the slit is $J_0 = 1/2$.

The integration in equation (A.8) is performed numerically in the complex plane of k , see appendix B. Then, after calculation of all the unknowns of the system of equation (A.5), the amplitudes of the waveguide cavity modes E_α, E'_α can be found. All the amplitudes of the modes in the dielectric regions ‘1, 2, 4, 5’ are expressed in terms of the amplitudes E_α, E'_α and thus, energy fluxes can be computed. For instance, the amplitudes t_k

$$t_k = \frac{1}{f_{k45}^+} \sum_\gamma E'_\gamma \langle k | \beta \rangle, \quad (\text{A.13})$$

are related to the Poynting vector $\mathbf{S} = \frac{1}{2} \text{Re}(\mathbf{E} \times \mathbf{H}^*)$ flux $J_5 = \lim_{z \rightarrow \infty} \int dx S_z$ as follows

$$J_5 = \frac{1}{2} \sum'_k Z_{k5} |t_k|^2, \quad (\text{A.14})$$

where the prime implies the summation over the propagating states only. Then using relation (A.13), the transmission coefficient $T = J_5/J_0$ can be written as

$$\begin{aligned} T &= \sum_{\gamma, \gamma'} G_{\gamma\gamma'}^T E'_\gamma E_{\gamma'}'^*, \\ G_{\gamma\gamma'}^T &= \sum_k \frac{Z_{k5}}{|f_{k45}^+|^2} \langle \gamma | k \rangle \langle k | \gamma' \rangle. \end{aligned} \quad (\text{A.15})$$

Appendix B. Green’s function numeric integration

The integration inside the tensor $G_{\alpha\alpha'}$ in equation (A.8) presents evident problems due to the presence of the poles on the real axis of k . The physical origin of the poles given

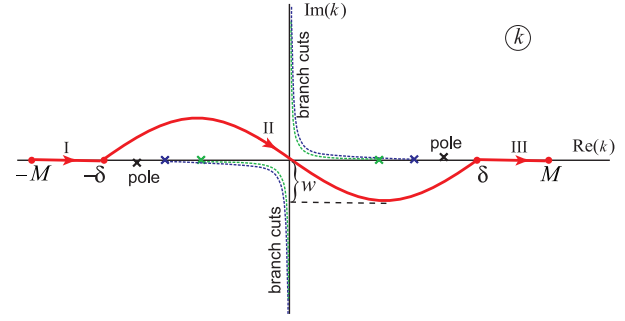


Figure B.1. The schematic representation of the integration path in the complex plane k of the x -component of the wavevector. The infinitesimally small absorption is ‘switched on’ in order to represent the branch cuts.

by $f_{kln}^- = 0$ is attributed to the DWMs of the layers ‘2’ and ‘4’, see figure A.1. In order to prevent the integration of the singularity, the integration path should be modified continuing analytically the integrand into the complex plane of the variable k . According to Cauchy’s theorem, the value of the integral is not affected by the integration path if the deformation of the initial path does not lead to the crossing of the pole and the branch cuts. The branch points correspond to the vanishing of the z -components of the wavevectors in the dielectric media, $k_{zl} = 0$. Thus, the integration path can be chosen as is shown in figure B.1.

Denoting the integrand by the function $F(k)$, the integral reads

$$I = \int_{-\infty}^{\infty} dk F(k) \simeq \int_{-M}^M dk F(k), \quad (\text{B.1})$$

where the integration inside the infinite limits is approximated by the integral in a finite domain of size $2M$. Then the integration path shown in figure B.1 can be split into 3 parts, and inside each part the path is parameterized $k_j = k_j(t)$ ($j = \text{I, II, III}$) so that the integration is reduced to the domain $[0, 1]$:

$$I \simeq \sum_j \int_0^1 dt F[k_j(t)] \frac{dk_j}{dt}, \quad (\text{B.2})$$

where

$$\begin{aligned} k_{\text{I}}(t) &= -M + (M - \delta)t, \\ k_{\text{II}}(t) &= -\delta + 2\delta t + iw \sin(2\pi t), \\ k_{\text{III}}(t) &= \delta + (M - \delta)t, \end{aligned} \quad (\text{B.3})$$

where the parameters M, δ and w are chosen so that the best convergency of the integrals is provided. The integral over t is performed using Simpson’s rule.

References

- [1] Schroter U and Heitmann D 1998 *Phys. Rev. B* **58** 15419
- [2] Porto J A, García-Vidal F J and Pendry J B 1999 *Phys. Rev. Lett.* **94** 2845

- [3] Collin S, Pardo F, Teissier R and Pelouard J L 2002 *J. Opt. A: Pure Appl. Opt.* **4** S154–60
- [4] Lee K G and Park Q H 2005 *Phys. Rev. Lett.* **95** 103902
- [5] Moreau A, Lafarge C, Laurent N, Edee K and Granet G 2007 *J. Opt. A: Pure Appl. Opt.* **9** 165–9
- [6] Sturman B, Podivilov E and Gorkunov M 2008 *Phys. Rev. B* **77** 075106
- [7] Martín-Moreno L, García-Vidal F J and Pendry J B 2004 *Science* **305** 847–8
- Martín-Moreno L, García-Vidal F J and Pendry J B 2005 *J. Opt. A: Pure Appl. Opt.* **7** S97–101
- [8] Hibbins A P, Evans B R and Sambles J R 2005 *Science* **308** 670–72
- [9] García de Abajo F J and Sáenz J J 2005 *Phys. Rev. Lett.* **95** 233901
- [10] Moreno E, Martín-Moreno L and García-Vidal F J 2006 *J. Opt. A: Pure Appl. Opt.* **8** S94–7
- [11] García-Vidal F J, Lezec H J, Ebbesen T W and Martín-Moreno L 2003 *Phys. Rev. Lett.* **90** 213901
- [12] Wang C M, Huang H I, Chao C C, Chang J Y and Sheng Y 2007 *Opt. Express* **15** 3496–501
- [13] Hendry E, García-Vidal F J, Martín-Moreno L, Gómez Rivas J, Bonn M, Hibbins A P and Lockyear M J 2008 *Phys. Rev. Lett.* **100** 123901
- [14] Li Z-B, Yang Y-H, Kong X-T, Zhou W-Y and Tian J-G 2008 *J. Opt. A: Pure Appl. Opt.* **10** 095202
- [15] Martín-Moreno L, García-Vidal F J, Lezec H J, Degiron A and Ebbesen T W 2003 *Phys. Rev. Lett.* **90** 167401
- [16] García-Vidal F J, Martín-Moreno L, Lezec H J and Ebbesen T W 2003 *Appl. Phys. Lett.* **83** 4500
- [17] Wang C, Du C and Luo X 2006 *Phys. Rev. B* **74** 245403
- [18] Lin D Z, Chang C K, Chen Y C, Yang D L, Lin M W, Yeh J T, Liu J M, Kuan C H, Yeh C S and Lee C K 2006 *Opt. Express* **14** 3503–11
- [19] Lin D-Z, Cheng T-D, Chang C-K, Yeh J-T, Liu J-M, Yeh C-S and Lee C-K 2007 *Opt. Express* **15** 2585–91
- [20] Liu Y, Shi H, Wang C, Du C and Luo X 2008 *Opt. Express* **16** 4487–93
- [21] Jackson D R, Chen J, Qiang R, Capolino F and Oliner A A 2008 *Opt. Express* **16** 21271–81
- [22] Moreno E, Fernández-Domínguez A I, Ignacio Cirac J, García-Vidal F J and Martín-Moreno L 2005 *Phys. Rev. Lett.* **95** 170406
- [23] Christensen J, Fernandez-Dominguez A I, de Leon-Perez F, Martín-Moreno L and García-Vidal F J 2007 *Nat. Phys.* **3** 851–2
- [24] Lu M-H, Liu X-K, Feng L, Li J, Huang C-P, Chen Y-F, Zhu Y-Y, Zhu S-N and Ming N-B 2007 *Phys. Rev. Lett.* **99** 174301
- [25] Nikitin A Yu, García-Vidal F J and Martín-Moreno L 2009 *Appl. Phys. Lett.* **94** 063119
- [26] Schouten H F, Visser T D, Lenstra D and Blok H 2003 *Phys. Rev. E* **67** 36608